The strenous state of the contact at the sliding - flip pairs

Odhisea Koça[1], Anis Sulejmani[2], Klodian Dhoska[3]
Polytechnic University of Tirana, Albania
Email: odisekoca2008@hotmail.com[1], anissulejmani@gmail.com[2], kdhoska@upt.al[3]

Abstract: *The exact determination of strain on the load application area, regards to changing material or shape is one of the main problems of the mini structure constructions, which it does not interfere with the classical methods of linear elasticity. The main purpose of this article is to demonstrate accomplishments in the knowledge of linear elasticity with different mathematical methods, in order to penetrate into the area or into the contact lining, taking into consideration the friction between the bodies in contact. The methods and hypotheses are related to the analysis of different classical half-plane problems in loads of different types of linear elasticity. This material shows a clear original solution of the strained state in the contact area including the surface lining; it serves as a solution to the various contact plan problems. The details and the elements of the vehicles are part of a broad field, which should be optimized considering different analytical solutions and using various computer programs. These solutions can be installed in their structure. Classical methods in the details apply only when the hypotheses on studied subjects are being met, such as Material Resistance studying the Rod. A detail with a length of ten times greater than the transverse dimension. That's the reason why extreme problems or problems out of the different hypotheses are solved and proven in practice with the most creative and sophisticated methods. The solution given in this article is an important contribution to constructive calculations, which is also associated with other works carried out by me on the friction coefficient on the flip-flop slippery contact.*
Keywords*: STRINGS, ELLIPTICAL COORDINATES, CONTACT HERZIT, CONTACTLESS CONTACT, SURFACE CONTACT*

1. Subplant loaded with normal and tangential loads

The Fig. 1 depict a normal and tangential load in half planes.

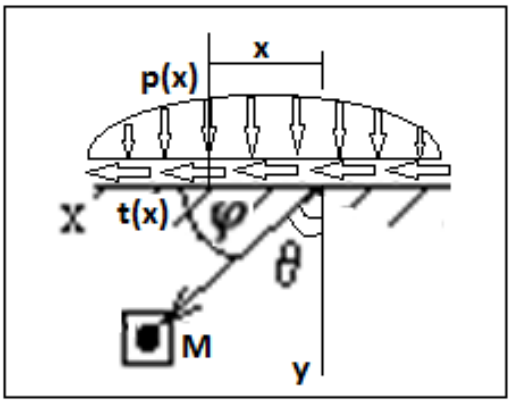

Fig.1 *Normal and tangential load in half planes*

For the most appropriate normal load is to be shifted to a bi-harmonic function F(z) and then to the harmonic functions Φ and Ψ where $F(z) = \Phi + y \cdot \Psi$ and $z = x + i \cdot y$. The strains from the strain relief will be [1-3].

$$\sigma_{xx} = \frac{\partial^2 F}{\partial y^2}; \sigma_{yy} = \frac{\partial^2 F}{\partial x^2}; \sigma_{xy} = -\frac{\partial^2 F}{\partial x \partial y}$$

Knowing that the harmonic functions satisfy the condition

$$\nabla^2 \Phi = \frac{\partial^2 \Phi}{\partial x^2} + \frac{\partial^2 \Phi}{\partial y^2} = 0, \text{ we get}$$

$$\Psi = -\frac{\partial \Phi}{\partial y};\ \varphi = \frac{\partial \Psi}{\partial y} \rightarrow \varphi = -\frac{\partial^2 \Phi}{\partial y^2} = \frac{\partial^2 \Phi}{\partial x^2} \quad (1)$$

Afterward we get:

$$\sigma_{xx} = \frac{\partial^2 F}{\partial y^2} = \varphi + y \cdot \frac{\partial \varphi}{\partial y}; \sigma_{yy} = \frac{\partial^2 F}{\partial x^2} = \varphi - y \cdot \frac{\partial \varphi}{\partial y};\ \sigma_{xy} = -\frac{\partial^2 F}{\partial x \partial y} = -y \cdot \frac{\partial \varphi}{\partial x} \quad (2)$$

After collecting normal strains, the first strain tensor invariant will be:

$$\varphi = \frac{\sigma_{xx} + \sigma_{yy}}{2} \quad (3)$$

The most convenient tangential load is to go to a bi-harmonic function as below:

$$F(z) = \Phi + x \cdot \Psi, \text{ ku } z = x + i \cdot y. \quad (4)$$

Strengths from strain solution will be:

$$\sigma_{xx} = \frac{\partial^2 F}{\partial y^2} = \psi - x \cdot \frac{\partial \psi}{\partial x}; \sigma_{yy} = \frac{\partial^2 F}{\partial x^2} = \psi + x \cdot \frac{\partial \psi}{\partial x};\ \sigma_{xy} = -\frac{\partial^2 F}{\partial x \partial y} = -x \cdot \frac{\partial \psi}{\partial y};\ \psi = \frac{\sigma_{xx} + \sigma_{yy}}{2} \quad (5)$$

In the case of normal and tangential load these functions will be as below:

$$\varphi = -P \cdot \frac{\sin\theta}{\pi \cdot r}; \psi = -T \cdot \frac{\cos\theta}{\pi \cdot r};\ \bar{F}(z) = \varphi + i \cdot \psi = -\frac{1}{\pi \cdot r}(P \cdot \sin\theta + i \cdot T \cdot \cos\theta) \quad (6)$$

when P = T group together into the complex variable z

$$\bar{F}(z) = -\frac{P \cdot i}{\pi \cdot z} = -\frac{P \cdot i}{\pi \cdot r \cdot e^{i \cdot \theta}} = -\frac{P \cdot i \cdot e^{-i \cdot \theta}}{\pi \cdot r} = -\frac{P \cdot i \cdot (\cos\theta - i \cdot \sin\theta)}{\pi \cdot r}. \quad (7)$$

In the case when the P and T forces are located at the 'u' distance from the origin we have:

$$\bar{F}(z) = \frac{P \cdot i}{\pi \cdot (u - z)}. \quad (8)$$

In case of distributed load we will integrate:

$$\bar{F}(z) = \int \frac{p(u) \cdot i}{\pi \cdot (u - z)} du \quad (9)$$

where φ is the real part of $\bar{F}(z)$ and ψ is the imaginary part of $\bar{F}(z)$.

For normal load we have:

$$\sigma_{xxN} = \varphi + y \cdot \frac{\partial \varphi}{\partial y}; \sigma_{yyN} = \varphi - y \cdot \frac{\partial \varphi}{\partial y};\ \sigma_{xyN} = -y \cdot \frac{\partial \varphi}{\partial x} \quad (10)$$

For the tangential load we have:

$$\sigma_{xxT} = \psi - x \cdot \frac{\partial \psi}{\partial x} = 2 \cdot \psi - \sigma_{xyN}; \sigma_{yyT} = \psi + x \cdot \frac{\partial \psi}{\partial x} = \sigma_{xyN};\ \sigma_{xy} = -x \cdot \frac{\partial \psi}{\partial y} = \sigma_{xxN} \quad (11)$$

2. The usage of elliptical coordinates

In the x and y axes system, we have different functions such as strains, deformations, and displacements, which are very complicated. The differential equations that they have emerged may present different difficulties to be solved. Another system of axes is the elliptical coordinate's ξ, η. These functions can come up with simpler formulas as well as with the solution of the differential equations from which the equation have emerged to be lighter. Fig. 2 depict Elliptic coordinates in the contact problem.

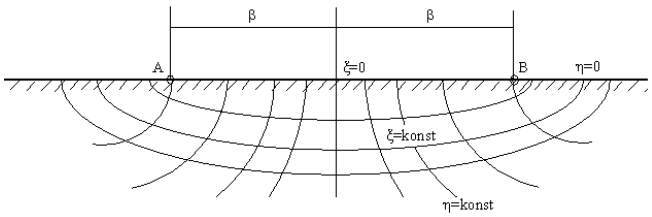

Fig.2 *Elliptic coordinates in the contact problem*

In the complex variable $z = x + i \cdot y$ or $\zeta = \xi + i \cdot \eta$ for the transformation

$$z = \beta \cdot \cosh \zeta = \beta \cdot \frac{e^{\zeta}+e^{-\zeta}}{2} = \beta \cdot \frac{e^{(\xi+i\eta)}+e^{-(\xi+i\eta)}}{2} = \beta \cdot \frac{e^{\xi}\cdot e^{i\cdot\eta}+e^{-\xi}\cdot e^{-i\cdot\eta}}{2}$$

$$x = \beta \cdot \cosh \xi \cdot \cos \eta \text{ dhe } y = \beta \cdot \sinh \xi \cdot \sin \eta$$

3. The integral solution for the symmetric term (Herc's fiery contact)

We analyze the case of contact with normal and tangential load according to the problem of Herc, see Fig. 3.

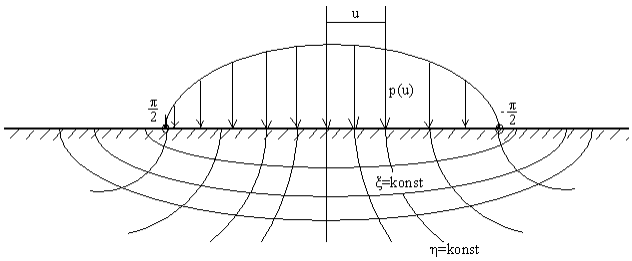

Fig.3 *Herculean contact in elliptical coordinates*

$$p(u) = C_1 \cdot \cos\theta = \frac{C_1}{\beta} \cdot \sqrt{\beta^2 - u^2} \; dhe \; u = -\beta \cdot \sin\theta \qquad (12)$$

From the mathematical analysis we draw:

$$\int \frac{\sqrt{\beta^2-u^2}}{u-z} du = \sqrt{\beta^2-u^2} - z \cdot \sin^{-1}\left(\frac{u}{\beta}\right) + \sqrt{z^2-\beta^2} \cdot \cos^{-1}\left(\frac{\beta^2-z\cdot u}{\beta\cdot(u-z)}\right) \qquad (13)$$

So we have the equation:

$$\bar{F}(z) = \frac{i}{\pi} \cdot \int \frac{p(u)\cdot du}{u-z} = \frac{i}{\pi} \cdot \int_a^b \frac{C_1\sqrt{\beta^2-u^2}}{\beta\cdot(u-z)} du = -C_1 \cdot i \cdot (\cosh\zeta - \sinh\zeta) = -C_1 \cdot i \cdot e^{-\zeta} = -C_1 \cdot i \cdot e^{-\xi} \cdot (i \cdot \cos\eta + \sin\eta) \qquad (14)$$

with its real and imaginative part:

$$\varphi = -C_1 \cdot e^{-\xi} \cdot \sin\eta \text{ dhe } \psi = -C_1 \cdot e^{-\xi} \cdot \cos\eta \qquad (15)$$

4. Sample preparation

In the case of rough rolling contact we have both pressure terms. We analyze the second term of pressure as it was first analyzed at Herc's contact, see Fig. 4.

$$p(u) = -C_2 \cdot \sin(2\cdot\theta) = 2 \cdot C_2 \cdot \frac{u}{\beta^2} \cdot \sqrt{\beta^2-u^2} \quad \text{and} \quad u = -\beta \cdot \sin\theta$$

We define the potential function for this pressure:

$$\int_a^b \frac{\sqrt{\beta^2-u^2}}{\beta\cdot(u-z)} \cdot u \cdot du = u \cdot \left[\sqrt{\beta^2-u^2} - z \cdot \sin^{-1}\left(\frac{u}{\beta}\right) + \sqrt{z^2-\beta^2} \cdot \cos^{-1}\left(\frac{\beta^2-z\cdot u}{\beta\cdot(u-z)}\right)\right] - \left[\frac{\pi\cdot\beta^2}{2} - \pi\cdot(\beta^2-z^2) - \pi\cdot(\beta+z)\cdot\sqrt{z^2-\beta^2}\right]_{-\beta}^{\beta} = \pi\cdot\beta^2 \cdot \frac{\sinh(2\cdot\zeta)-\cosh(2\cdot\zeta)}{2} = -\frac{\pi\cdot\beta^2}{2}\cdot e^{-2\cdot\zeta}$$

$$\bar{F}(z) = \frac{i}{\pi} \cdot \int_{-\beta}^{\beta} \frac{p(u)}{u-z} \cdot du = \frac{i}{\pi} \cdot \frac{2\cdot C_2}{\beta^2} \cdot \left(-\frac{\pi\cdot\beta^2}{2} \cdot e^{-2\cdot\zeta}\right) = -C_2 \cdot i \cdot e^{-2\cdot\zeta} \qquad (20)$$

and the formative reinforcement of functions:

$$\varphi = -C_2 \cdot e^{-2\cdot\xi} \cdot \sin(2\cdot\eta) \; ; \; \psi = -C_2 \cdot e^{-2\cdot\xi} \cdot \cos(2\cdot\eta) \qquad (21)$$

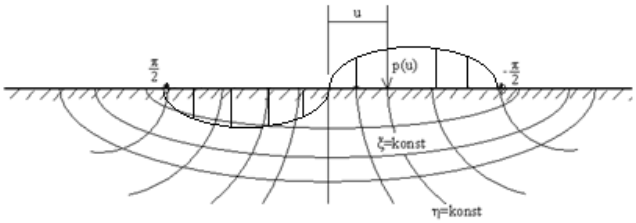

Fig.4 *Contact with antimetric term*

5. Strings on the lining of contact bodies

Laboratory The Fig. 5 depict a pressure at rolling contact for $\lambda = 0.424$.

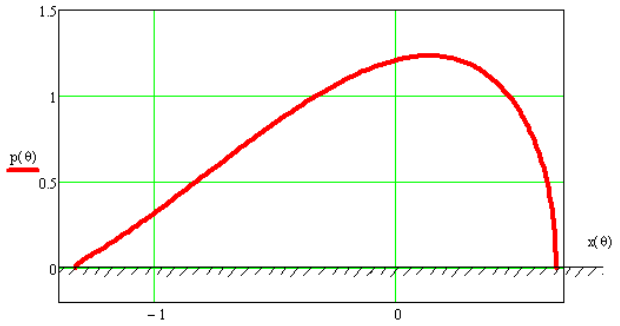

Fig.5 Pressure at rolling contact for $\lambda = 0.424$

In this case we have rotation (flip), so we have both terms, therefore the analytical solution will be:

$$p_n(\theta) = C_1 \cdot \cos\theta - 0.424 \cdot C_1 \cdot \sin(2\cdot\theta)$$

From reference pressure we have simplifications:

$$\overline{p_n(\theta)} = \frac{p_n(\theta)}{C_1} = \cos\theta - 0.424 \cdot \sin(2\cdot\theta) \; ; \; \bar{t} = \frac{t-\alpha}{\beta} = -\sin\theta \; [-90^0 \div 90^0]$$

In case of total slide we draw:

$p_t(\theta) = \mu \cdot [\cos\theta - 0.424 \cdot \sin(2\cdot\theta)]$; $\mu \rightarrow$ the coefficient of friction between the two bodies in contact

The contact surface in elliptical coordinates is divided into three parts. The CD part where $\eta = \pi$, the contact AB part, which depends directly on the oppressive force $\xi = 0$ and the part BD where $\eta = 0$.

Fig.6 *Surface of the bodies in contact and its elliptical variables*

When flipping in real contact, the most loaded case is realized when we have full slide. The reinforcements in this case for the lining will be:

Area CA: $\eta = \pi$ from Eq. (23), (25), (29), (30):

$$\sigma_{xx1N} = 0;\ \sigma_{xx1T} = 2 \cdot \mu \cdot C_1 \cdot \left(e^{-\xi}\right);\ \sigma_{xx2N} = 0;\ \sigma_{xx2T} = -2 \cdot \mu \cdot C_2 \cdot e^{-2\cdot\xi}$$

$$\sigma_{yy1N} = 0;\ \sigma_{yy1T} = 0;\ \sigma_{yy2N} = 0;\ \sigma_{yy2T} = 0$$

$$\sigma_{xy1N} = 0;\ \sigma_{xy1T} = 0;\ \sigma_{xy2N} = 0;\ \sigma_{xy2T} = 0$$

Area AB: $\xi = 0$ by ek (23), (25), (29), (30):

$$\sigma_{xx1N} = -C_1 \cdot \sin\eta;\ \sigma_{xx1T} = -2 \cdot \mu \cdot C_1 \cdot \cos\eta;\ \sigma_{xx2N} = -C_2 \cdot \sin(2 \cdot \eta);\ \sigma_{xx2T} = -2 \cdot \mu \cdot C_2 \cdot \cos(2 \cdot \eta)$$

$$\sigma_{yy1N} = -C_1 \cdot \sin\eta;\ \sigma_{yy1T} = 0;\ \sigma_{yy2N} = -C_2 \cdot \sin(2 \cdot \eta);\ \sigma_{yy2T} = 0$$

$$\sigma_{xy1N} = 0;\ \sigma_{xy1T} = -\mu \cdot C_1 \cdot \sin\eta;\ \sigma_{xy2N} = 0;\ \sigma_{xy2T} = -2 \cdot \mu \cdot C_2 \cdot \sin(2 \cdot \eta)$$

Zone BD: $\eta = 0$ by ek (23), (25), (29), (30):

$$\sigma_{xx1N} = 0;\ \sigma_{xx1T} = -2 \cdot \mu \cdot C_1 \cdot \left(e^{-\xi}\right);\ \sigma_{xx2N} = 0;\ \sigma_{xx2T} = -2 \cdot \mu \cdot C_2 \cdot e^{-2\cdot\xi}$$

$$\sigma_{yy1N} = 0;\ \sigma_{yy1T} = 0;\ \sigma_{yy2N} = 0;\ \sigma_{TyyTM} = 0$$

$$\sigma_{xy1N} = 0;\ \sigma_{xy1T} = 0;\ \sigma_{xy2N} = 0;\ \sigma_{xy2T} = 0$$

By analyzing the surface lining we distinguish in the passive body, the maximum strain at the trailing edge of the contact path which is equal to $\sigma_{1.max} = 2 \cdot (1 + \lambda) \cdot \mu \cdot p_H$. It is known that destruction starts at the points that are pulled and these are found at the ends of the contact path, see Fig. 7.

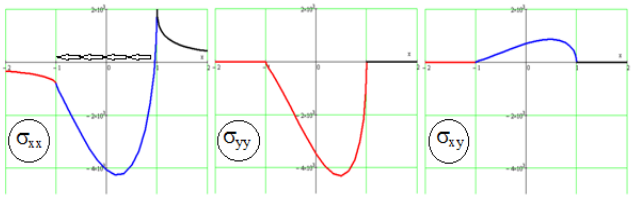

Fig.7 *Struts on the passive body surface lining in contact for case* $C_1 = 3500\ \frac{N}{mm^2}, \mu = 0.2$

By analyzing the surface lining we distinguish in the active body that the maximum retraction strain is located at the other end of the contact path with a smaller value $\sigma_{1.max} = 2 \cdot (1 - \lambda) \cdot \mu \cdot p_H$, see Fig. 8.

Fig.8 *Strands on the surface of the active body in contact with the case* $C_1 = 3500\ \frac{N}{mm^2}, \mu = 0.2$

6. The skeleton of the tooth at the toothed wheel

Skeleton is an injury from tiredness in contact with the tooth surface, is a progressive destruction of cyclic strains and has the features of fatigue destruction [4-6]. Oily wheels in the environment of oil are always damaged by the skull, especially this damage appears in the area from the pole to the toes. According to the coefficient of friction literature in this case (in oil environment) varies by type of oil at the limits 0.05÷0.06 [5]. When the oil is absent varies in the range of 0.09÷0.4, so the maximum tangential strain appears on the surface and the discussion ends. It starts the destruction of the fatigue contact.

In a couple of sprockets we distinguish the active wheel that the movements comes from and the passive wheel that the movement goes. In addition, we recognize the active tooth with the highest tangential velocity and the passive tooth with lower tangential velocity because the normal speed is the same. At the beginning of the active tooth, the active wheel is active and at the end of the gear the active tooth is active wheel. This helps us to set the direction of the friction forces, starting from the active tooth, always against it and the opposite tooth according to the principle of counteracting action.

Seeing the tangential speed game, we conclude that when the contact point is located on the part from the foot to the poly of the gear of each tooth of each wheel, the maximum tensile strengths in the traction are impacted by frictional forces. This strain is in tune and explains every disaster, especially from fatigue contact. From both bodies, one of them appears to be in charge, and this is in the tooth area up to the poly Fig.9 and Fig.10.

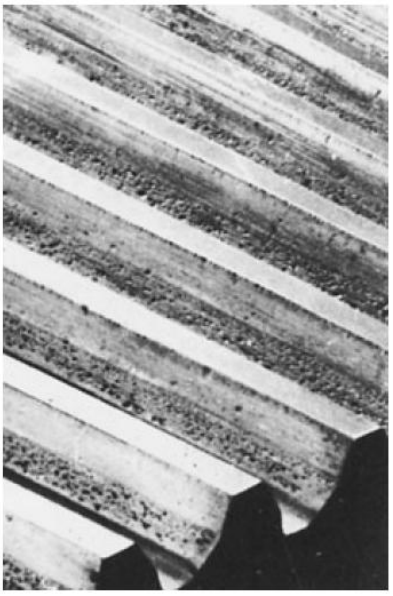

Fig. 9 *The skeleton in the wings of the teeth*

Active Wheels Active 1Passive Wheels Active Wheel 2Active wheel. Passive wheel

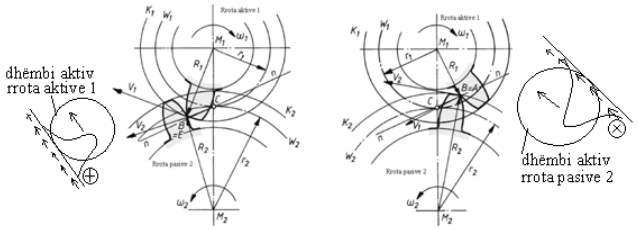

Fig.10 *Determining the frictional forces direction*

The maximum value of the pulled force for the passive tooth and the active tooth are respectively $\sigma_{1.pasiv.max} = 2 \cdot (1 + 0.424) \cdot \mu \cdot p_H$ and $\sigma_{1.aktiv.max} = 2 \cdot (1 - 0.424) \cdot \mu \cdot p_H$. Therefore, we conclude that the destruction always starts from the surface due to the friction and the tendency to flip the tooth.

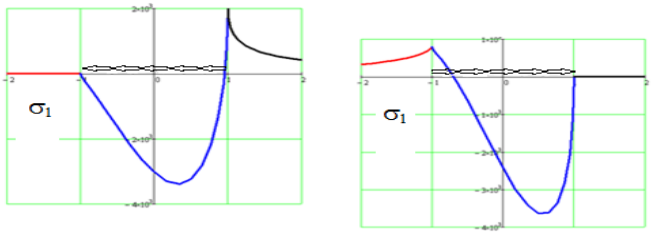

Fig.11 *Main strain on the body surface and counter-contact surfaces*

7. Conclusions

From the harshness of the rough contact and its application to the toothed wheel we conclude that:

- Analytical determination of stiff contact state.
- At the end of the contact line always appears a pulling strain due to friction.
- The passive body is loaded more in tow than the active body due to friction and flip.
- Friction is the main cause of the skirmish.
- The maximum peak strength on the surface lining depends directly on the friction coefficient and the Hercule pressure.
- The skeleton starts from the pole and goes straight to the end of the tooth because in this area the maximum peak pull strength $\sigma_s=2.848\cdot\mu\cdot p_H$ appears.
- Calculation of the tooth skeleton are merely calculation of fatigue contact.

References

1. P.P. Teoderescu. Probleme plane in teoria elasticitati 1. Bucuresti 1960

2. N.I. Bezuhov. Osnovi teori uprugosti, plastiçnosti i polzuçesti. Moskva 1960

3. N.Boicu. Contactul elastic linear. Bucuresti 1977

4. O.Koça, Uber Kontaktprobleme der Ebenen Elastizitatstheorie" Teil II . Referim. Laboratorium fur Techniche Mechanik. Universitat Paderborn (GH), Germany 07.1991

5. O.Koça, Analyse des Spannungszustandes fur Kontaktprobleme bei Abwalzung mit Gleiten. Anwendung dieser Theori auf Zahnräder" Referim. Laboratorium fur Techniche Mechanik. Universitat Paderborn (GH), Germany 1992

6. K. Dhoska, Tensile Testing Analysis of the HRB400 Steel Reinforcement Bar. International Journal of Innovative Technology and Interdisciplinary Sciences, 2019, 2(3), 253-258.